Wetland mapping from sparse annotations with satellite image time series and temporal-aware segment anything model

Shuai Yuan[a,b], Tianwu Lin[b], Shuang Chen[a], Yu Xia[b], Peng Qin[b], Xiangyu Liu[b], Xiaoqing Xu[b], Nan Xu[d],
Hongsheng Zhang[a], Jie Wang[b,1], Peng Gong[a,1]

[a]*Department of Geography, The University of Hong Kong, Hong Kong, China*
[b]*Pengcheng Laboratory, Shenzhen, China.*
[c]*Department of Electronics and Information Engineering, Harbin Institute of Technology (Shenzhen), Shenzhen, China*
[d]*Key Laboratory for Geo-Environmental Monitoring of Great Bay Area, Ministry of Natural Resources, Guangdong Key Laboratory of Urban Informatics, Shenzhen Key Laboratory of Spatial Smart Sensing and Services, Shenzhen University, Shenzhen, China*

Abstract

Accurate wetland mapping is critical for ecosystem monitoring and management, yet acquiring dense pixel-level annotations is prohibitively costly. In practice, only sparse point labels are typically available, and existing deep learning-based models struggle under such weak supervision. Meanwhile, wetlands exhibit strong seasonal and inter-annual dynamics, making single-date imagery insufficient and causing substantial omission and commission errors when mapping. Although powerful foundation models like the Segment Anything Model (SAM) provide promising generalization from point prompts, it is intrinsically designed for static natural images, resulting in spatially fragmented masks in heterogeneous wetland environments and cannot exploit satellite image time series. To address these challenges, we propose WetSAM, a novel SAM-based framework that effectively leverages satellite image time series to enhance wetland mapping from sparse point annotations. WetSAM adopts a dual-branch design: (1) The temporal branch is prompted by sparse point labels to extend the SAM with a hierarchical adapter and a dynamic temporal aggregation module. By decomposing time series into seasonal trends and transient events, this branch effectively distinguishes wetland features from phenological variations; (2) The spatial branch reconstructs distinct boundaries via a temporal-constrained region-growing strategy, iteratively expanding sparse points into reliable dense pseudo-labels; (3) A bidirectional consistency regularization enforces minimizing the discrepancy of the predictions from two segmentation heads of two branches. We validate the effectiveness of WetSAM across eight diverse global locations, each covering an area of around $5,000\ km^2$ and with various wetland types and geographical features. WetSAM reaches an average F1-score of 85.58%, considerably outperforming other state-of-the-art algorithms. Results demonstrate that WetSAM achieves accurate, structurally consistent segmentation from sparse labels. With minimal labeling effort, our framework shows strong generalization ability and holds promise for scalable, low-cost wetland mapping at high spatial resolutions.

Keywords: wetland mapping, satellite image time series, sparse annotation, segment anything model, temporal adaptation

---

[1]Corresponding author: penggong@hku.hk, wangj10@pcl.ac.cn

1. Introduction

Wetlands, as one of the world's most productive ecosystems, provide invaluable ecosystem services (Gong et al., 2010; Yuan et al., 2025b), including water balance regulation, carbon storage, and mitigation of global climate change (Zhang et al., 2021; Erwin, 2009; Pattison-Williams et al., 2018). However, accelerating climate change and human disturbances have led to widespread wetland degradation (Hu et al., 2017), creating an urgent need for accurate, efficient, and frequently updated wetland maps to support conservation and management (Yuan et al., 2025b; Team, 2025).

In this context, satellite remote sensing, with its unique advantages of synoptic coverage, multi-temporal capabilities, and periodic observations, has become an indispensable tool for large-scale wetland monitoring (Gong et al., 2010). From the decades-long historical archives provided by the Landsat series to the high spatiotemporal resolution data streams from modern satellite constellations like Sentinel and Gaofen (Murray et al., 2019; Wang et al., 2024), it is now possible to characterize both intra-annual and inter-annual wetland dynamics driven by seasonal hydrology and vegetation phenology. Nevertheless, despite their potential, current wetland mapping faces two major limitations that impede large-scale, high-resolution applications.

First, data-driven deep learning methods have been increasingly applied to wetland mapping using medium- to high-resolution satellite images (Hosseiny et al., 2021; Jamali et al., 2022). Such supervised models typically rely on dense pixel-level annotations, yet producing such labels for wetlands is prohibitively expensive and often infeasible. Unlike many man-made objects with well-defined edges (Yuan et al., 2024), wetland boundaries are inherently gradual, blurry, and spatially heterogeneous, reflecting transitional zones between aquatic and terrestrial environments. As a result, manual pixel-wise annotations across large areas are labor-intensive and not scalable (Liu et al., 2025). In practice, the most realistic form of annotation is sparse point labels, where annotators mark representative wetland and non-wetland locations without attempting to delineate uncertain boundaries (Yuan et al., 2025a). However, such point-level supervision provides extremely limited spatial information and does not directly encode object extent or boundary geometry (Chan et al., 2025). Under this setting, existing weakly supervised segmentation models are fundamentally constrained: while sparse points can guide the model toward the semantic identity of wetlands, they offer little supervision on wetland boundaries, often leading to fragmented predictions when applied to complex and heterogeneous wetland landscapes (Hua et al., 2021; Xu & Ghamisi, 2022).

Second, wetlands exhibit strong temporal dynamics, and single-date imagery is insufficient for reliable classification (Yuan et al., 2025b). Seasonal inundation, temporary flooding, and phenological changes can cause wetlands to appear spectrally similar to uplands during dry periods, or vice versa (Figure 1). A single snapshot only captures the transient appearance of wetlands rather than their temporal features. Incorporating time-series imagery is therefore essential, as it enables the full seasonal trajectory to reveal the characteristic dynamics of wetlands and resolve ambiguities. Although time-series deep learning models can exploit temporal information, they typically rely on full pixel-level supervision, and how to effectively incorporate such rich time-series information under sparse supervision remains largely unexplored (Garnot & Landrieu, 2021). For example, most existing multi-temporal deep learning models for wetland mapping are trained with dense pixel-
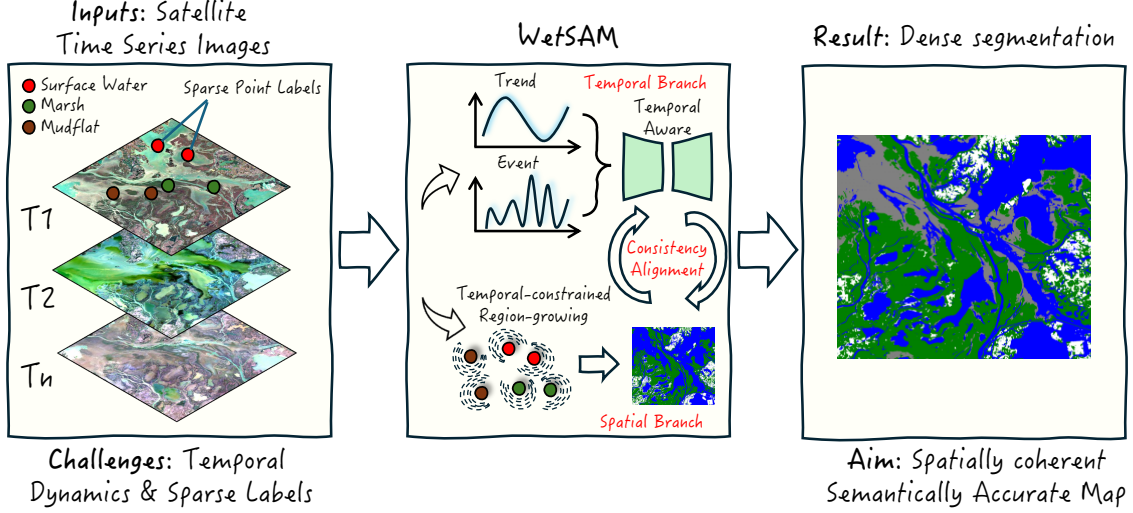
Figure 1: Overview. We propose an end-to-end, single- stage model for wetland mapping from satellite image time series under sparse point supervision. Note the difficulty of semantic segmentation of wetlands from a single image, highlighting the need for modeling temporal dynamics and spatial contexts.

level annotations, while learning temporal representations from sparse point labels has received little attention (Hosseiny et al., 2021; Marjani et al., 2025).

Recently, vision foundation models such as the Segment Anything Model (SAM) (Kirillov et al., 2023) have emerged as a promising solution to mitigate annotation costs by generating segmentation masks from point prompts. However, directly applying SAM to wetland mapping exposes two critical limitations. (1) SAM is trained on natural images and struggles with the complex patterns in satellite imagery, leading to spatially fragmented masks when prompted with sparse points (Zhang et al., 2025). (2) Wetlands exhibit diverse temporal behaviors: slow-varying phenological trends and abrupt hydrological events. Standard SAM is inherently static and cannot model temporal signatures, and existing adaptations fail to decouple these two distinct temporal frequencies, leading to confusion between temporary inundation and permanent wetland features. As a result, SAM cannot reliably delineate wetlands nor exploit their characteristic seasonal trajectories. These limitations highlight a critical research gap: No existing framework can simultaneously learn from sparse point annotations and leverage satellite image time series for accurate wetland mapping, nor effectively adapt SAM to the temporal and spectral features of remote sensing imagery.

To bridge this gap, we propose WetSAM, a novel end-to-end framework designed to effectively leverage satellite image time series to accurately map dynamic wetlands only under sparse point-level supervision (Figure 1). Specifically, WetSAM consists of three key modules. The **temporal branch** extends SAM by introducing a hierachical adapter and a novel dynamic temporal aggregation module, which decomposes satellite image time series into low-frequency phenological trends and high-frequency hydrological events, enabling SAM to capture the complex temporal characteristics of wetlands under the guidance of sparse point annotations and to effectively distinguish between stable wetland core areas and seasonal transition zones. The **spatial branch** addresses the limited spatial coverage of sparse supervision by transforming region growing from a fixed post-processing step into a supervision generation mechanism. Starting from

3

sparse point annotations, a temporal-constrained region-growing strategy is used to progressively generate dense pseudo labels, which provide structured supervision for learning spatially complete wetland boundaries in an end-to-end manner. These pseudo-labels provide the model with far richer supervisory information than the original sparse points. Finally, a **bidirectional prediction alignment** ensures the predictions from the two branches are guided to be mutually reinforcing and aligned, ultimately enabling the model to learn to generate wetland boundaries that are both accurate and structurally coherent.

The main contributions of this study are as follows:

- We propose WetSAM, the first framework that integrates sparse point supervision with satellite image time series for wetland mapping. By jointly leveraging spatial and temporal cues within a unified design, WetSAM alleviates the two major challenges of wetland mapping, i.e., extremely limited annotations and pronounced seasonal dynamics, without requiring dense labels.

- We adapt and extend the Segment Anything Model (SAM) to satellite image time series processing. A temporal adaptation branch extracts wetland phenological features from time series imagery, while a spatial branch generates reliable dense supervision via a temporal-constained region-growing strategy. A bidirectional consistency regularization further aligns temporal and spatial predictions, enabling accurate and structurally coherent segmentation from sparse labels.

- We demonstrate the scalability and generalization ability of WetSAM across eight diverse wetland regions globally. Extensive experiments show that WetSAM substantially outperforms existing baselines under minimal annotation cost, providing a practical and cost-effective solution for high-resolution wetland mapping at regional to global scales.

The rest of this paper is organized as follows. Related work of this study is introduced in Section 2. Section 3 illustrates WetSAM in detail. Section 4 introduces the study areas and materials in this work. Section 5 shows the experimental results. Ablation studies and discussions are presented in Section 6. Conclusions are summarized in Section 7.

2. Related Work

2.1. Wetland mapping using satellite remote sensing imagery

Wetland mapping via satellite remote sensing has evolved from traditional image processing to machine and deep learning. Early methods relying on handcrafted features and spectral indices (Xu et al., 2018; Ashok et al., 2021; Dong et al., 2014) were interpretable but sensitive to atmospheric and spectral variations. Subsequent approaches, including rule-based strategies (Dronova, 2015; Ruan & Ustin, 2012), object-based analysis (Wang et al., 2023b), and spectral unmixing (Hong et al., 2021; Sidike et al., 2019), addressed some limitations but often lacked generalization and required manual parameterization. Machine learning algorithms, such as SVM (Lin et al., 2013) and random forests (Mahdianpari et al., 2017), later improved accuracy and flexibility by modeling nonlinear relationships (Jing et al., 2020). However, these methods remain dependent on representative training samples and are limited in exploiting time-series information (Yuan et al., 2025b).

Due to powerful feature representations, deep learning has since emerged as the dominant approach, providing remarkable capabilities for automatic feature extraction and large-scale mapping. Convolutional and fully convolutional networks (Pouliot et al., 2019; Li et al., 2022), together with region-proposal methods such as Mask R-CNN (Guirado et al., 2021) and Transformer-based architectures (Jamali & Mahdianpari, 2022), have demonstrated clear advantages in handling high-resolution data, preserving complex boundaries, and integrating multi-source information. These advances have significantly raised the accuracy ceiling for wetland classification and segmentation. For example, Ma et al. (2022) proposed cascaded R-CNN model to detect the dike-ponds with manual regular boundaries. Jamali & Mahdianpari (2022) combined Swin transformer and deep CNN for complex coastal wetland classification.

Yet, despite their success, two fundamental limitations remain unresolved. First, current deep learning frameworks rely heavily on dense, pixel-level annotations for supervision. Such labels are prohibitively expensive to acquire for wetlands, where boundaries are often fuzzy, transitional, and context-dependent. In practice, point-level annotations are far easier to obtain (Wang et al., 2023b; Zhang et al., 2024), but existing models are ill-equipped to learn effectively from such sparse supervision. Second, wetlands exhibit strong seasonal and inter-annual dynamics driven by hydrology and vegetation phenology, therefore single-date imagery often fails to capture these dynamics. Although time-series deep learning models have shown the ability to extract temporal patterns (Garnot & Landrieu, 2021; Marjani et al., 2025), they rely on dense supervision and are therefore unsuitable for the sparse-label setting common in wetland mapping.

These two limitations directly motivate the development of new frameworks that can both unlock the value of sparse point annotations and explicitly model temporal dynamics.

2.2. SAM in remote sensing

Recent advances in vision foundation models, particularly the Segment Anything Model (SAM), have created new opportunities to reduce annotation cost (Kirillov et al., 2023). SAM can generate segmentation masks from simple prompts such as points or boxes, demonstrating impressive generalization across natural images. Numerous studies have been conducted to further explore the capabilities of SAM and to apply it effectively across diverse task scenarios (Ma et al., 2024; Yan et al., 2023; Chen et al., 2023; Zhang et al., 2023a).

However, its potential may be constrained in certain domain-specific conditions (Zhang et al., 2023b; Ali et al., 2025). To address this limitation, SAM can be adapted or fine-tuned with even a single example of a new class or object to improve its performance. Building on this idea, multiple studies have fine-tuned or adapted SAM to enhance its effectiveness in remote sensing tasks. For example, Zhou et al. (2024) proposed Multiscale Enhanced SAM (MeSAM), a fine-tuning strategy tailored to remote sensing images that adapts SAM for semantic segmentation tasks and improves its segmentation accuracy on such data. Wang et al. (2023a) leveraged SAM and existing remote sensing object detection datasets to construct an efficient pipeline for generating a large-scale remote sensing segmentation dataset SAMRS. Yan et al. (2023) introduced RingMo-SAM, a foundation model for multimodal remote sensing image segmentation, capable of segmenting both optical and SAR data while also identifying object categories. This highlights SAM's potential for deployment

in remote sensing applications while reducing the need for extensive manual annotation.

However, wetlands are highly dynamic ecosystems shaped by seasonal hydrology, climate variability, and human disturbance. While such dynamics are critical for reliable wetland delineation, SAM is fundamentally designed as a single-image foundation model and lacks native mechanisms to model temporal dependencies. As a result, single-date predictions are often insufficient to characterize intra-annual variability and periodic wetland transitions. Even though SAM 2 and SAM 3 (Ravi et al., 2024; Carion et al., 2025) support temporal inputs, they are primarily designed for continuous visual observations such as videos, where temporal coherence is dense and object identities evolve smoothly across frames. Satellite image time series, by contrast, are typically sparse and irregular, and are subject to strong seasonal, atmospheric, and sensor-induced variability, which challenges the core assumptions of video-based temporal modeling and limits their applicability to dynamic wetland mapping.

Moreover, in practical wetland mapping, supervision is often limited to sparse point annotations. Although SAM supports point prompts for mask generation, its prompt-to-mask paradigm is primarily driven by local appearance similarity and assumes relatively coherent object structures (Kirillov et al., 2023). Recent studies have shown that, when applied to remote sensing imagery, such point-prompted segmentation frequently produces spatially fragmented or globally inconsistent masks, especially in heterogeneous and densely structured scenes (Subhani, 2025). This limitation is particularly evident in wetland environments. Wetlands exhibit strong spatial heterogeneity, gradual transitions, and blurred boundaries (Dronova et al., 2015). Under the sparse supervision, relying solely on point prompts lacks the constrains for the boundary, resulting in spatially fragmented masks. These observations suggest that directly applying SAM to wetland mapping remains challenging without additional mechanisms to enforce spatial consistency.

Consequently, the central challenge addressed in this study is how to effectively leverage temporal information and sparse point annotations to map spatially coherent and semantically accurate wetland extents. To this end, we propose WetSAM, an end-to-end framework that extents SAM to integrate time-series information with iterative spatial refinement, enabling reliable wetland mapping from satellite image time series under sparse point supervision.

3. WetSAM

3.1. Problem definition

Let $\mathcal{X} = \{x_t\}_{t=1}^T$ denote a satellite image time series, where $x_t \in \mathbb{R}^{H \times W \times C}$ is the image at time t. Let $\mathcal{P} = \{(p_i, l_i)\}_{i=1}^N$ be the set of sparse point labels, where $p_i \in \Omega = \{1, \ldots, H\} \times \{1, \ldots, W\}$ are the spatial coordinates and $l_i \in \{0, 1, ..., K\}$ is the corresponding class label for one of K wetland categories. Critically, the number of annotated points N is significantly smaller than the total number of pixels ($N \ll H \times W$), framing our task as a weakly-supervised learning problem.

Our goal is to train a network, parameterized by θ, which functions as a mapping $f_\theta : \mathbb{R}^{T \times H \times W \times C} \rightarrow \{0, 1, ..., K\}^{H \times W}$. This network takes the entire image time series $\mathcal{X}$ as input and outputs a dense semantic segmentation map $\mathcal{M} = f_\theta(\mathcal{X})$. Since the dense ground-truth mask is unavailable during training, the model's

parameters θ can only be optimized by minimizing a loss function evaluated at the sparse annotation locations. The objective is formally defined as:

$$\min_{\theta} \mathbb{E}_{(\mathcal{X}, \mathcal{P})} \left[\frac{1}{N} \sum_{i=1}^{N} \mathcal{L}_{\text{ce}}(f_{\theta}(\mathcal{X})[p_i], l_i) \right], \tag{1}$$

where $f_{\theta}(\mathcal{X})[p_i]$ denotes the model's predicted probability distribution at the spatial coordinate p_i, and $\mathcal{L}_{\text{ce}}$ is the standard cross-entropy loss.

Solving this objective presents two fundamental challenges that directly correspond to the core problems identified in wetland mapping: First, the function f_{θ} must effectively learn to aggregate information from the entire time series $\mathcal{X}$ to make a correct prediction at a single point p_i. This requires the model to comprehend the complex phenological patterns and temporal features of different wetland types, merely from sparse supervisory signals. Second, the training loss is computed only on a very small subset of pixels, which means propagating the semantic information from these sparse points $\mathcal{P}$ to the entire, unlabeled image to generate a spatially coherent and structurally complete segmentation map $\mathcal{M}$.

Our proposed method, WetSAM, is designed to explicitly address these two challenges within a unified dual-branch framework, including a temporal branch, a spatial branch, and a consistency regularization in between as detailed in the following sections. The overall framework of WetSAM is presented in Figure 2.

3.2. Temporal branch: enabling SAM time-aware

Although SAM demonstrates strong generalization from point prompts, it is inherently designed for static natural images and cannot exploit the rich temporal cues present in satellite image time series1. As a result, SAM fails to capture the characteristic phenological patterns of wetlands, which are essential for distinguishing wetland categories from seasonal inundation or spectral ambiguities2. To enable SAM to interpret temporal dynamics under sparse supervision, we design a two-level temporal adaptation strategy that (1) adapts SAM to remote sensing imagery and (2) models wetland temporal contexts explicitly.

Hierarchical multi-scale adapter. Wetland remote sensing imagery exhibits unique spectral mixtures, moisture-driven reflectance changes, and fine-scale vegetation-water boundaries that SAM is not originally designed for. Meanwhile, wetland appearance varies substantially across seasons, making both shallow textures and deep semantics important. Existing adapter designs for remote sensing mainly target simple objects and are insufficient for wetlands, which contain high intra-class variability. To address this, we integrate a hierarchical multi-scale adapter into SAM's encoder. Shallow layers focus on enhancing fine-scale boundary cues, while deeper layers refine temporally varying semantic patterns. As shown in Figure 2 (b1) and (b2), for each timestamp t, the shallow adapter takes the feature map and applies (1) global pooling and two shared MLPs for spectral re-weighting, (2) global pooling and a 5×5 convolution for capturing contextual patterns, and (3) a bottleneck structure to reduce the dimensionality of the feature map. The deep adapter takes the feature map and applies a single 3×3 convolution with a scaled dot-product attention mechanism to efficient semantic refinement. Together, these hierarchical adapters align SAM's representation space with remote sensing characteristics.
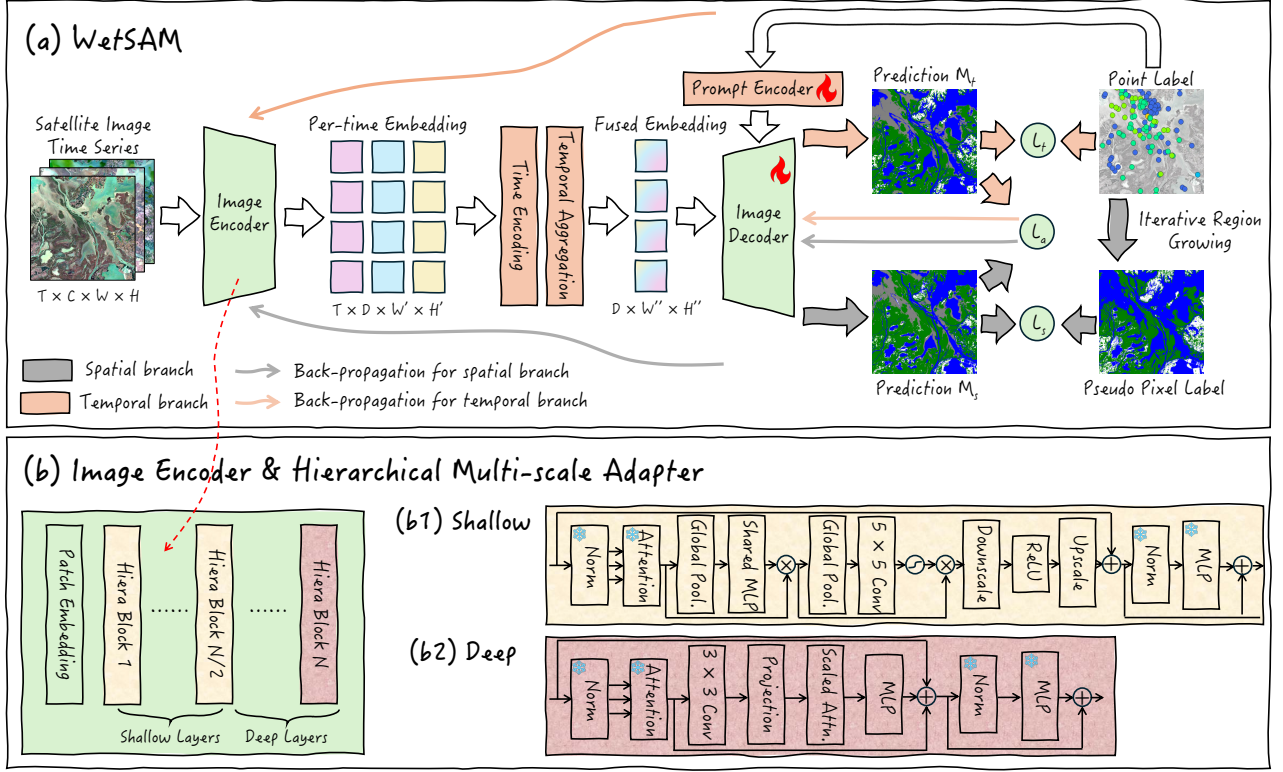
Figure 2: The WetSAM framework. (a) is the overview of the framework. (b) is the detailed architecture of the Encoder.

Dynamic temporal contexts awareness. After extracting representations $\{F_t\}_{t=1}^{T}$ for each timestamp through the hierarchical adapter, we further incorporate explicit temporal positional information to model the phenological evolution of wetlands. Since different time points exhibit distinct seasonal patterns, encoding temporal position is essential for distinguishing wetland dynamics driven by seasonal cycles. For each timestamp t, we first introduce a sinusoidal positional embedding E_t as follows:

$$E_t^{(2i)} = sin(\frac{t}{10000^{\frac{2i}{D}}}), \quad E_t^{(2i+1)} = cos(\frac{t}{10000^{\frac{2i}{D}}}), \tag{2}$$

where i indexes the embedding dimension. This formulation produces a continuous and periodic representation of time, enabling the model to naturally capture annual hydrological cycles. The time-aware feature at timestamp t is then computed as $\tilde{F}_t = F_t + E_t$.

To effectively aggregate the temporal sequence $\{\tilde{F}_t\}_{t=1}^{T}$ into a comprehensive wetland representation, we design a temporal aggregation module inspired by the idea of trend–remainder decomposition in STL (Cleveland et al., 1990), but implement it in a learnable and end-to-end manner. The module separates the time series into low-frequency seasonal trends and high-frequency transient fluctuations as shown in Figure 3 (a). First, we employ a learnable smoothing operation to extract the trend signal E_{trend}. This is implemented via a 1D depth-wise convolution, which acts as an adaptive low-pass filter as described:

$$E_{low} = \text{Conv1d}_{smooth}(\{\tilde{F}_t\}_{t=1}^{T}). \tag{3}$$

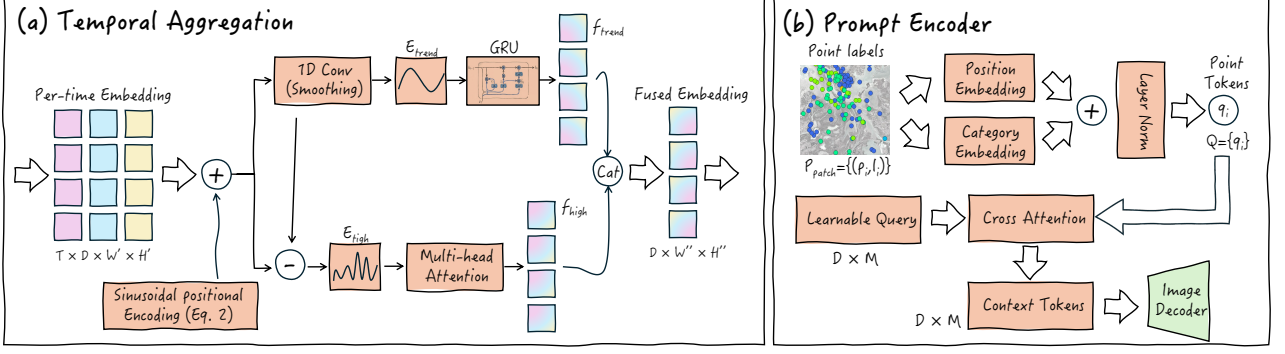This trend signal represents the smooth, continuous evolution of vegetation phenology or water level changes.

Figure 3: The temporal aggregation module.

The residual between the original sequence and the trend serves as the high-frequency component E_{high}, capturing rapid fluctuations such as sudden flooding or abrupt environmental changes $E_{high} = \tilde{F} - E_{trend}$ The two components are then processed to capture distinct temporal features. For the trend component E_{trend}, we employ a Gated Recurrent Unit (GRU) (Chung et al., 2014) to model the sequential dependencies and the overall shape of the phenological curve, compressing it into a trend embedding f_{low}.

The high-frequency component E_{high} captures sudden reflectance changes such as flooding, rainfall events, or human interventions, etc. These signals are sparse and irregular, making them well-suited for attention-based modeling. We adopt a multi-head temporal attention mechanism, where each attention head specializes in identifying a distinct subset of critical transient events. For each attention head h, we compute attention weights α_h as:

$$\alpha_h = softmax(\frac{q_h^\top K_h}{\sqrt{d_k}}), \tag{4}$$

where K_h is the Key matrix projected from E_{high}, and q_h is a learnable query vector. The head-specific event feature is computed as the attention-weighted sum:

$$o_h = \sum_t \alpha_h[t]V_h[t]. \tag{5}$$

The weighted sum of the Value matrix V_h yields a feature vector focusing on key events. The outputs of all heads are concatenated to form the final high-frequency feature:

$$f_{high} = Concat(o_1, o_2, ..., o_H). \tag{6}$$

Finally, the global representation is obtained by concatenating the trend and event features

$$f_{fused} = Concat(f_{low}, f_{high}). \tag{7}$$

We should note that, unlike the standard SAM, which uses category-agnostic point prompts, our weakly supervised setting provides both spatial locations and semantic categories. As shown in Figure 3 (b), let $\mathcal{P}_{patch} = \{(p_i, l_i)\}_{i=1}^{N_p}$ denote the annotated points within a patch. Each point is encoded into a class-aware token:

$$q_i = \text{LayerNorm}\big(e^{pt}(p_i) + e^{cls}(l_i)\big), \tag{8}$$

where $e^{pt}(\cdot)$ and $e^{cls}(\cdot)$ denote positional and category embeddings, respectively. This yields a set of point tokens $Q = \{q_i\}_{i=1}^{N_p}$. To handle the variable number of point annotations, we aggregate Q into a fixed-length context representation using attention pooling. Specifically, a set of M learnable latent queries $Z \in \mathbb{R}^{D \times M}$ attends to Q via a cross-attention, producing context tokens $C \in \mathbb{R}^{D \times M}$ that summarize the semantic distribution of annotated wetlands within the patch. We retain the architecture of the SAM decoder while adapting its interaction pattern for dense semantic segmentation. Instead of using prompts to query image features, we treat the fused time-aware image features f_{fused} as queries and the context tokens C as keys and values within the decoder:

$$F_{\text{dec}} = Decoder_{\text{SAM}}(f_{\text{fused}}, C). \tag{9}$$

This allows each spatial location to attend to the global semantic context provided by sparse annotations, resulting in a dense feature map F_{dec} for subsequent multi-class prediction.

3.3. Spatial branch: iterative boundary refinement

To complement the semantic discrimination provided by the temporal branch and to enable effective learning of spatial structures under sparse supervision, we introduce a spatial branch that explicitly incorporates region-growing–based pseudo supervision into the training process as Figure 2 shows. It consists of a learnable expanded prediction head that is trained using dense pseudo labels generated by a temporal-constraint region growing strategy. This branch leverages spatial autocorrelation, where spatially adjacent pixels with similar temporal features are likely to belong to the same wetland type, while preventing the error propagation commonly observed in static expansion. Given two pixels u and v with time-series profiles $x_u, x_v \in \mathbb{R}^{T \times C}$, we measure their temporal similarity using cosine similarity:

$$\rho(u,v) = \frac{x_u \cdot x_v}{\|x_u\|_2 \|x_v\|_2}. \tag{10}$$

This metric focuses on the shape of phenological trajectories rather than absolute reflectance magnitude. A pixel is assimilated only if it exhibits a highly coherent seasonal trajectory with the seed point (i.e., $\rho > \tau$), thereby suppressing leakage into spectrally similar but semantically different regions. To prevent noise amplification in early training, the first stage performs conservative region growing strictly from ground-truth points $\mathcal{P}_{gt}$:

$$M_{\text{spat}}^{(0)} = \text{Grow}(\mathcal{P}_{gt}, \tau), \tag{11}$$

yielding a high-precision initial mask. As the temporal branch becomes more reliable, its predictions provide incremental guidance to densify spatial supervision. Specifically, at the end of every K training epochs, unlabeled pixels with high-confidence temporal predictions are extracted as pseudo-seeds:

$$\mathcal{P}_{\text{pseudo}} = \{u \mid \max(f_{\text{temp}}(u)) > 0.95\}. \tag{12}$$

To further reduce confirmation bias, these seeds are retained only if their predicted class is spatially consistent with their 3×3 neighborhood. The merged seed set $\mathcal{P}_{\text{total}} = \mathcal{P}_{gt} \cup \mathcal{P}_{\text{pseudo}}$ enables a refined region

growing process:

$$M_{\text{spat}}^{(k)} = \text{Grow}\big(\mathcal{P}_{\text{total}}, \tau\big). \tag{13}$$

The region growing procedure itself is non-differentiable and does not participate in backpropagation. It serves solely as a pseudo-label generator that expands sparse point annotations into dense supervision maps. These expanded labels are then used to supervise a dedicated expanded prediction head, enabling the spatial branch to be trained end-to-end despite the non-differentiable nature of the region growing process. This expansion is performed locally around the newly added pseudo-seeds to ensure efficiency. The updated map $M_{\text{spat}}^{(k)}$ serves as the dense pseudo-label supervision for the subsequent training period. Through this iterative feedback loop, the density of reliable seeds increases over time, significantly shortening propagation distances and progressively sharpening boundaries. Consequently, the spatial branch continually suppresses early-stage noise and enhances structural consistency as the model converges.

3.4. Prediction alignment: consistency regularization

Based on the shared decoder feature map, we employ two parallel prediction heads corresponding to two complementary supervision pathways: a temporal head and a spatial head. Both heads are instantiated as 1×1 convolutional layers that project the D-dimensional decoder features into K-class logits.

The *temporal head*, denoted as f_{temp}, is supervised by sparse point-level annotations and focuses on learning reliable semantic categorization driven by temporal dynamics. It produces a dense probability map

$$p_{\text{temp}} = \sigma\big(f_{\text{temp}}(F_{\text{dec}})\big), \tag{14}$$

where σ denotes the softmax function.

The *spatial head*, denoted as f_{spat}, is supervised by dense pseudo labels generated through the iterative region-growing process and focuses on capturing spatial continuity and complete object structures. It produces

$$p_{\text{spat}} = \sigma\big(f_{\text{spat}}(F_{\text{dec}})\big). \tag{15}$$

The temporal head is anchored by the high-confidence sparse annotations $\mathcal{P}_{gt}$, and is optimized using a point-wise cross-entropy loss:

$$\mathcal{L}_t = -\frac{1}{|\mathcal{P}_{gt}|} \sum_{(p,l) \in \mathcal{P}_{gt}} \log p_{\text{temp}}^{(p,l)}. \tag{16}$$

In contrast, the spatial head learns from the dense pseudo-labels $M_{\text{spat}}^{(k)}$ produced at iteration k of region growing. To mitigate class imbalance and boundary noise, we employ the Lovász-Softmax loss:

$$\mathcal{L}_s = \mathcal{L}_{\text{Lovasz}}\big(p_{\text{spat}}, M_{\text{spat}}^{(k)}\big). \tag{17}$$

Although the two heads share the same underlying representation, they are driven by complementary supervision signals with different reliability and coverage. To couple their learning dynamics and to regularize the influence of noisy pseudo-labels, we follow (Xu & Ghamisi, 2022) to introduce a prediction alignment loss that enforces consistency between their dense probability maps:

$$\mathcal{L}_a = \frac{1}{H \times W} \sum_{i=1}^{H \times W} \big\| p_{\text{temp}}^{(i)} - p_{\text{spat}}^{(i)} \big\|_2^2. \tag{18}$$

The overall training objective is given by:

$$\mathcal{L}_{total} = \mathcal{L}_t + \mathcal{L}_s + \lambda_a \mathcal{L}_a, \tag{19}$$

where λ_a controls the strength of the alignment regularization.

4. Study area and material

4.1. Study area

To comprehensively evaluate the effectiveness of the proposed WetSAM framework, we conduct experiments across eight selected study areas distributed on different continents with different wetland landscapes (Figure 4): 1) Poyang Lake, China (PL); 2) Mississippi River, United States (MR); 3) Sundarbans, India & Bangladesh (SD); 4) Sudd Wetland, South Sudan (SW); 5) Amazon, Brazil (AM); 6) Biesbosch, Netherlands (BS); 7) Pantanal, Brazil (PT); 8) Bayanbulak, China (BA).

These regions are chosen based on the following considerations: First, they encompass a broad range of wetland ecosystems across different climatic zones and continents, thereby providing a comprehensive and representative testbed for evaluating WetSAM. The study areas span tropical humid regions, subtropical monsoon regions, temperate maritime zones, arid continental basins, and equatorial savanna regions, ensuring exposure to diverse atmospheric and illumination conditions. Correspondingly, these regions have multiple kinds of wetlands, including mudflats, coastal mangroves, river-fed marshes, and seasonally inundated swamps, etc. Such ecological and geographical diversity allows us to comprehensively assess the model's robustness and generalization ability across different wetland landscapes. Second, these regions exhibit distinct temporal patterns. Some areas experience seasonal inundation cycles (PL, MR, PT), while others maintain relatively stable wetland conditions throughout the year (SD, BS). These contrasting phenological and hydrological trajectories are essential for evaluating the model's capability to capture different wetland dynamics. Third, each region covers a large area with around 5,000 km^2, which captures significant spatial heterogeneity and representativeness, providing a challenging setting for testing segmentation performance under sparse point supervision.

4.2. Material

A Sentinel-2 Level-2A time-series dataset is used in this study to support wetland mapping across the eight selected regions. Sentinel-2 provides multi-spectral bands ranging from visible to shortwave infrared with spatial resolutions of 10–60 m, delivering rich spectral information for monitoring vegetation, water bodies, soil moisture, and inland/coastal hydrological processes. All data is acquired from the Sentinel-2 Surface Reflectance Harmonized collection on Google Earth Engine (GEE) for the period from January 1, 2022 to December 31, 2023, covering two full hydrological cycles for each region. To ensure high-quality observations, we apply a two-stage cloud filtering strategy. First, Sentinel-2 scenes were filtered using the metadata field, retaining only images with cloud cover less than 20% within each study region. Second, we apply a pixel-level cloud and cirrus mask using the QA60 quality assurance band. Cloud and cirrus flags are removed via bitwise
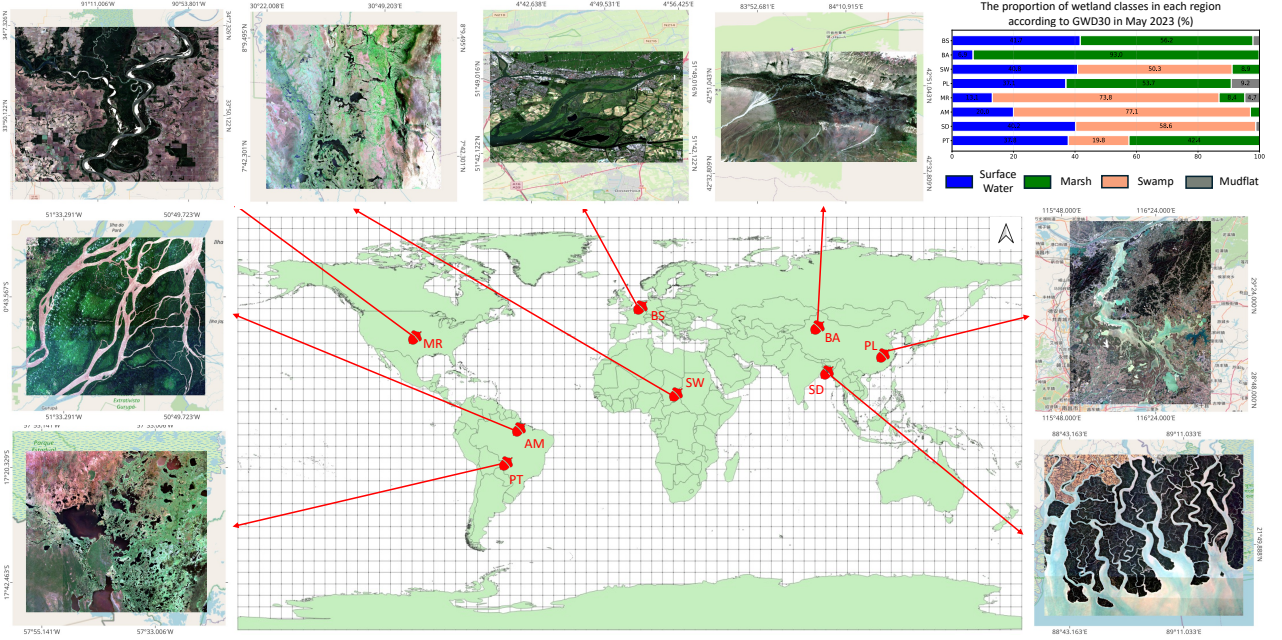
Figure 4: The study areas in our study, including 1) Poyang Lake, China (PL); 2) Mississippi River, United States (MR); 3) Sundarbans, India & Bangladesh (SD); 4) Sudd Wetland, South Sudan (SW); 5) Amazon, Brazil (AM); 6) Biesbosch, Netherlands (BS); 7) Pantanal, Brazil (PT); 8) Bayanbulak, China (BA). The sub-figure on the top right denotes the distributions of wetland classes in each region based on GWD30 (Team, 2025).

masking. After cloud masking, three bands with 10-m resolution are preserved for analysis: B2 (Blue), B3 (Green), B4 (Red). For each study region, a median composite is generated from all available cloud-free images to produce 12 representative monthly synthetic images.

Additionally, high-resolution Google Earth images and corresponding Sentinel-2 images are used to annotate and validate the point labels. We focus on four major classes, including surface water, swamp, marsh, and mudflat. We manually label approximately 2,000-4,000 points for each study area, with balanced representation across classes. Points are uniformly distributed within each of the eight study areas to avoid spatial overlap. Figure 5 summarizes the detailed sample information.
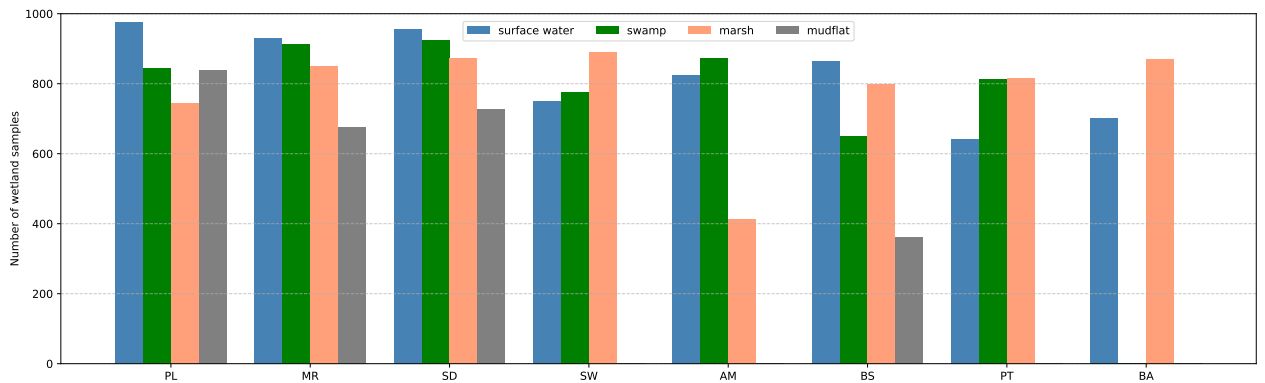

Figure 5: The number of wetland samples of each study area.

5. Experiments and evaluation

5.1. Experiment settings

All models are trained on the weakly supervised setting, where only point-based annotations are used as supervision. During training, each time-series image is cropped into 256×256 patches, and the corresponding sparse points (and their region-grown expansions) within each patch serve as the supervision signals for the spatial and temporal branches of WetSAM. We adopt an 8:2 split of the image patches for training and validation.

Training is performed using the PyTorch framework with four NVIDIA GeForce RTX 4090 GPUs for 50 epochs. The batch size is set to 8. The initial learning rate is 1×10^{-5} with a weight decay of 4×10^{-5}, and AdamW is used as the optimizer. Standard data augmentation techniques, including random flipping and rotation, are applied to enhance data diversity. During training, the SAM image encoder is kept frozen to preserve the pretrained structural priors of SAM under weak supervision. The hierarchical adapters, temporal aggregation module, conditioning injection layers in the decoder, as well as both the two segmentation heads are trained end-to-end. For evaluation, independent annotated points are used solely as the test set to quantitatively assess the performance of WetSAM under sparse supervision.

We use three common metrics to evaluate the performance of WetSAM, i.e., Precision, Recall, and F1-score. The mathematical definition of these metrics are:

$$Precision = \frac{1}{N} \sum_{n=1}^{N} \frac{TP}{TP + FP} \tag{20}$$

$$Recall = \frac{1}{N} \sum_{n=1}^{N} \frac{TP}{TP + FN} \tag{21}$$

$$F1\text{-}score = \frac{1}{N} \sum_{n=1}^{N} \frac{2TP}{2TP + FP + FN} \tag{22}$$

5.2. Results of WetSAM

We first evaluated the overall segmentation performance of WetSAM across the eight study regions. Figure 6 summarizes the global mean Precision, Recall, and F1-score. Under sparse point-level supervision, WetSAM achieves an average F1-score of 85.58%, an average Precision of 85.26%, and an average Recall of 86.64%. The consisent performance in eight study areas and three metrics demonstrates that WetSAM is able to recover the full spatial extent of wetland patches while maintaining accurate boundary delineation, despite being trained solely on sparse annotations.

Across individual regions, WetSAM shows stable and robust performance under diverse hydrological and climatic conditions. In stable wetland environments such as Sundarbans (SD) and Biesbosch (BS), WetSAM achieves powerful results with an average F1-score of 86.43%. In strongly seasonal regions such as Poyang Lake (PL), Sudd wetland (SW), and Pantanal (PT), WetSAM maintains a competitive average F1-score of 84.39%. Even though there is a slight decrease in these dynamic areas, the performance remains consistently high despite substantial seasonal transitions. This demonstrates WetSAM's superior ability to resolve temporal spectral ambiguity and handle seasonal hydrological fluctuations by effectively balancing precision and recall.
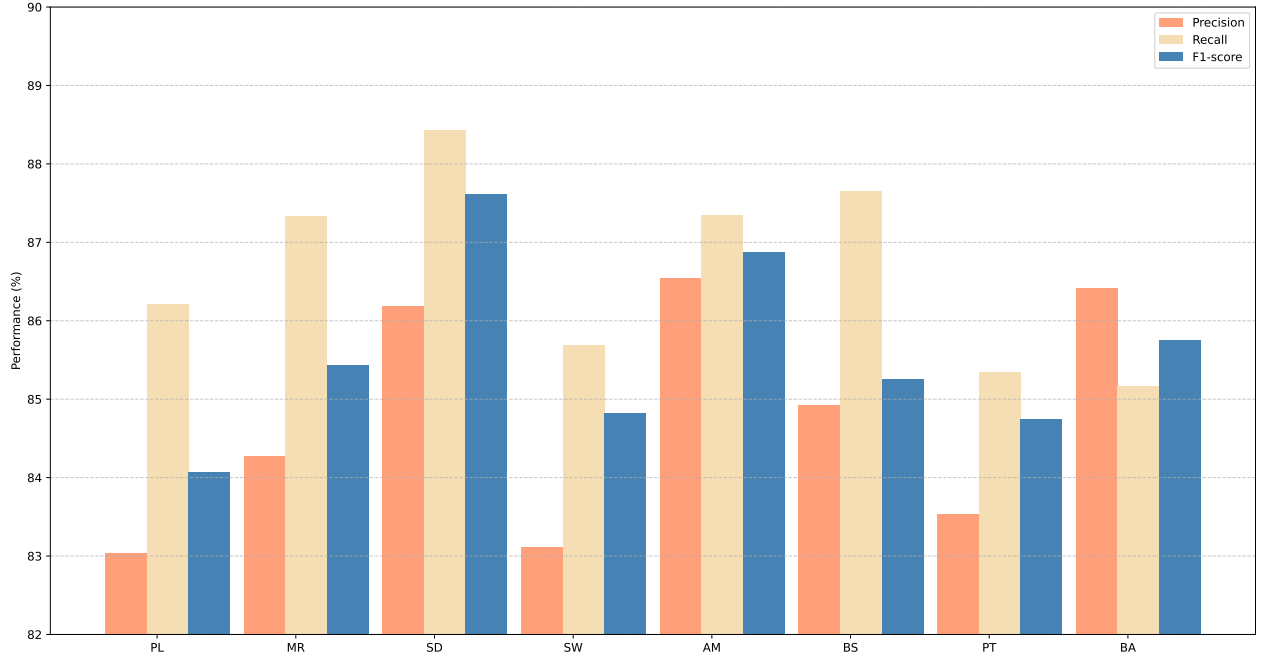
Figure 6: The performance of WetSAM in eight study areas, regarding three metrics, i.e., Precision, Recall, and F1-score.

We further report the performance by wetland type in Table 1, focusing on surface water, marsh, swamp, and mudflat. Surface water achieves the highest accuracy among all classes, reflecting its distinctive spectral response and relatively stable seasonal behavior. Marsh, swamp and mudflat show slightly lower but still robust performance, which is affected by their mixed vegetation–water composition and more complex phenological dynamics. Regional variability also corresponds well with known ecological differences. For example, SD and BS, where wetland conditions remain relatively stable throughout the year, exhibit uniformly high accuracy across surface water, marsh, swamp, and mudflat. In contrast, highly seasonal systems such as PL and PT show mildly reduced accuracy in vegetated and transitional wetland types, reflecting the stronger intra-annual variability and more complex boundary dynamics in these regions. BA, which lacks swamp and mudflat classes, maintains strong performance in surface water and marsh due to its relatively homogeneous landscape structure.

Figure 7 presents representative qualitative results produced by WetSAM across the study regions. The maps exhibit smooth and coherent wetland boundaries, including in fragmented transition zones (e.g., SW, PL) where spatial structures are typically complex. Fine-scale wetland features, including narrow water channels (e.g., AM, MR), small marsh areas (e.g., PT), and spatially sparse wetland patches (e.g., SW, PL), are clearly preserved, indicating strong sensitivity to detailed spatial patterns. Overall, the visualization results align with the quantitative results and demonstrate that WetSAM can generate spatially continuous, structurally meaningful, and temporally stable segmentation outcomes under sparse supervision.

Table 1: Type-level mapping performance (Precision / Recall / F1-score, %) of WetSAM across all eight study regions.

Region	Surface Water	Marsh	Swamp	Mudflat
PL	86.24 / 89.41 / 87.80	83.84 / 87.01 / 85.40	81.84 / 85.01 / 83.39	80.24 / 83.41 / 81.79
MR	87.48 / 90.53 / 88.98	85.08 / 88.13 / 86.58	83.08 / 86.13 / 84.58	81.48 / 84.53 / 82.98
SD	89.39 / 91.63 / 90.50	86.99 / 89.23 / 88.10	84.99 / 87.23 / 86.10	83.39 / 85.63 / 84.50
SW	85.61 / 88.19 / 86.88	83.11 / 85.69 / 84.38	80.61 / 83.19 / 81.88	–
AM	89.04 / 89.85 / 89.44	86.54 / 87.35 / 86.94	84.04 / 84.85 / 84.44	–
BS	88.13 / 90.85 / 89.47	85.73 / 88.45 / 87.07	83.73 / 86.45 / 85.07	82.13 / 84.85 / 83.47
PT	86.04 / 87.84 / 86.93	83.54 / 85.34 / 84.43	81.04 / 82.84 / 81.93	–
BA	87.92 / 86.67 / 87.29	84.92 / 83.67 / 84.29	–	–
Average	87.48 / 89.37 / 88.41	84.97 / 86.86 / 85.90	82.76 / 85.10 / 83.91	81.81 / 84.60 / 83.19

5.3. Comparative studies

We benchmark WetSAM against a comprehensive set of baseline methods, and a brief introduction is as follows. The original SAM (Kirillov et al., 2023) serves as prompt-driven foundation models capable of zero-shot segmentation but without temporal modeling. The SAM 2 (Ravi et al., 2024) supports temporal inputs with continuous visual observations. DINO-SAM (Zamboni et al., 2025) enhances SAM with self-supervised DINO features to improve mask quality in complex scenes. PSPNet (Zhao et al., 2017) represents classical semantic segmentation with pyramid pooling for multi-scale context aggregation, while SegNext (Guo et al., 2022) introduces a lightweight yet effective design for high-resolution segmentation tasks. CRGNet (Xu & Ghamisi, 2022) is a weakly-supervised segmentation method using sparse point annotations. UTAE (Garnot & Landrieu, 2021) is a temporal encoder–decoder model tailored for satellite image time series, capable of learning temporal dynamics but requiring dense supervision. Together, these baselines provide a diverse and representative comparison for evaluating WetSAM under sparse annotation settings.

All baseline results are summarized in Table 2. It should be noted that while most methods are trained directly with sparse point labels, the traditional semantic segmentation models (PSPNet, SegNext, and UTAE) are supervised by pseudo pixel labels expanded from the sparse points using the region-growing algorithm.

Overall, WetSAM achieves the highest F1-score among all methods, reaching an average of 85.58%. Across individual regions, WetSAM consistently yields strong and robust performance, maintaining F1-scores between 84% and 88%. This includes stable wetland environments such as SD and BS, as well as more dynamic systems like PL and SW. In highly seasonal regions (PL, SW, and PT), where substantial intra-annual flooding and vegetation changes typically increase segmentation difficulty, WetSAM maintains a clear advantage over all other baselines.

The foundation models (SAM, DINO-SAM, and SAM 2) demonstrate promising results, but their performance remains limited in heterogeneous wetland environments. SAM 2, which incorporates a memory attention mechanism for temporal propagation, achieves a significant improvement over the original SAM with an average F1-score of 83.15%. However, it still falls short of WetSAM, as its general-purpose memory mechanism lacks explicit modeling for domain-specific phenological trends. Traditional models like PSPNet and SegNext show lower and less stable performance, as they are heavily sensitive to the noise and boundary
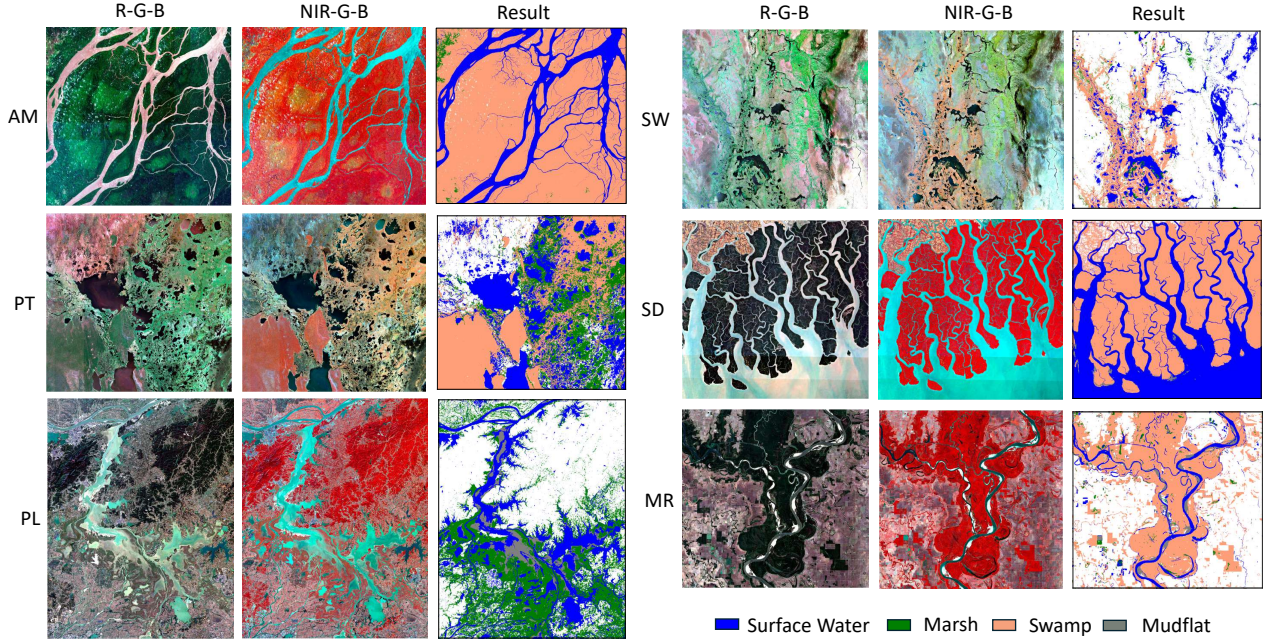
Figure 7: The visualization results of WetSAM.

Table 2: Comparison of F1-score (%) across eight study regions for all baseline methods and WetSAM.

Method	Type	PL	MR	SD	SW	AM	BS	PT	BA	Average
SAM (Kirillov et al., 2023)	Foundation model	78.14	80.21	82.55	76.12	79.34	80.01	75.22	77.89	78.69
SAM 2 (Ravi et al., 2024)	Foundation model	81.54	83.02	85.12	82.11	84.45	83.05	82.54	83.37	83.15
DINO-SAM (Zamboni et al., 2025)	Foundation model	80.26	82.35	84.41	78.36	81.55	82.47	76.98	79.54	80.74
PSPNet (Zhao et al., 2017)	Traditional DL model	72.31	75.44	77.12	70.08	73.66	74.52	68.32	72.11	73.21
SegNext (Guo et al., 2022)	Traditional DL model	73.12	76.11	78.23	71.21	74.22	75.91	69.11	73.02	74.37
CRGNet (Xu & Ghamisi, 2022)	Weakly supervised	77.01	79.12	81.33	75.05	78.14	79.22	73.45	76.33	77.46
UTAE (Garnot & Landrieu, 2021)	Temporal model	79.34	81.45	83.22	77.11	80.56	81.12	76.12	78.41	79.67
WetSAM	Ours	84.07	85.44	87.61	84.82	86.87	85.25	84.74	85.75	85.58

errors present in the pseudo-pixel labels. The temporal model UTAE performs relatively well in dynamic environments but is limited by the quality of the pseudo-supervision, resulting in moderate accuracy.

Taken together, these results demonstrate that WetSAM achieves consistently high and robust segmentation accuracy across diverse wetland ecosystems. The performance gap between WetSAM and strong baselines like SAM 2 and UTAE highlights the benefits of jointly temporal dynamics modeling and spatial continuity under sparse annotation settings. Figure 8, Figure 9, and Figure 10 provide the visualization results of these comparative studies.

6. Discussion

6.1. Effectiveness of modules in WetSAM

To further analyze the contributions of each component in WetSAM, we perform a series of ablation experiments to validate the effectiveness of the proposed modules for accurate wetland mapping under sparse
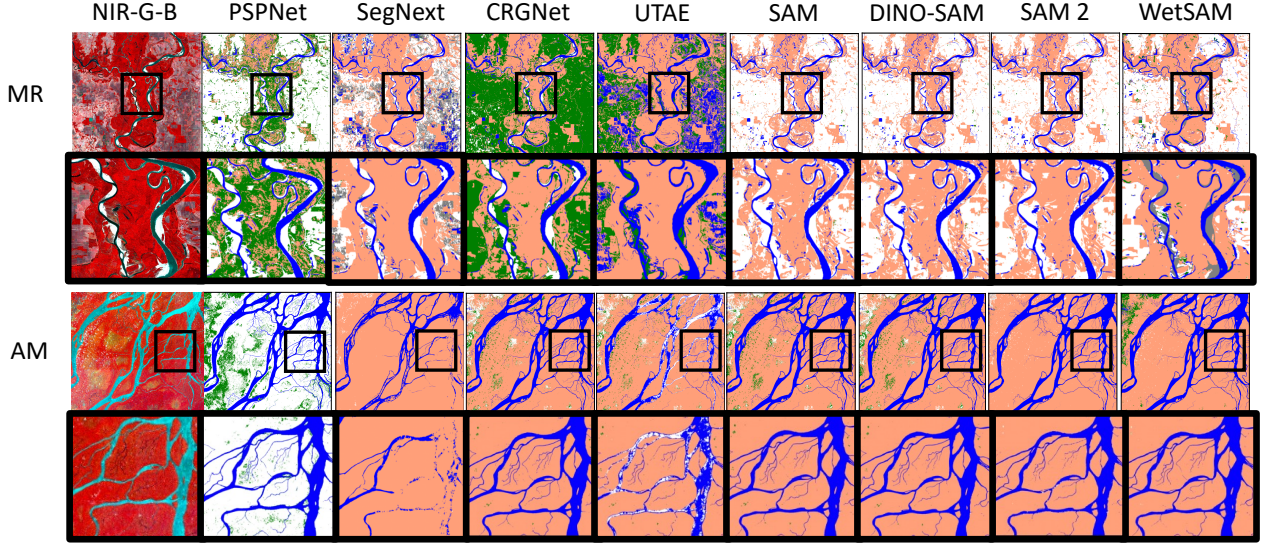
Figure 8: The visualization results of comparative studies.

supervision. Below, we detail the impacts of removing each module, and the results are shown in Table 3.

Rational for the temporal branch. Removing the temporal branch results in a model relying solely on spatial features from single-date imagery. In this configuration, the model fails to capture seasonal hydrological cycles essential for discriminating complex wetland types. As shown in Table 3, this leads to the significant performance degradation across all regions, with the average F1-score dropping from 85.58% to 79.51%. The largest decreases occurred in highly dynamic regions such as PL, SW, and PT, confirming that temporal context is the indispensable cornerstone for resolving spectral ambiguities caused by seasonal variability.

Rational for the spatial branch. Removing the spatial branch and the region-growing mechanism means the model loses the ability to propagate sparse point annotations into coherent spatial structures. Without dense pseudo-labels for supervision, the model suffers a drop in F1-score to 83.87%. The segmentation tends to degenerate into scattered predictions around annotated points. However, as observed in Table 3, the performance drop is less severe than that of removing the temporal branch. This suggests that while SAM's internal spatial priors can aggregate some similar features, the explicit spatial branch is still crucial for reconstructing complete wetland shapes from sparse inputs.

Rational for the prediction alignment. To evaluate the necessity of enforcing consistency between branches, we remove the prediction alignment loss and trained both branches independently. Quantitatively, the average F1-score fell to 84.61%. Without this mutual regularization, the spatial branch became sensitive to region-growing noise, while the temporal branch failed to benefit from the enriched spatial structures. This highlights the importance of prediction alignment as a bidirectional knowledge distillation mechanism that harmonizes the semantic precision of the temporal branch with the structural completeness of the spatial branch.

Rational for multi-scale adapter. Removing the hierarchical multi-scale adapter forces the model to use the original SAM encoder without spectral adaptation. Since the original SAM is designed for natural images,
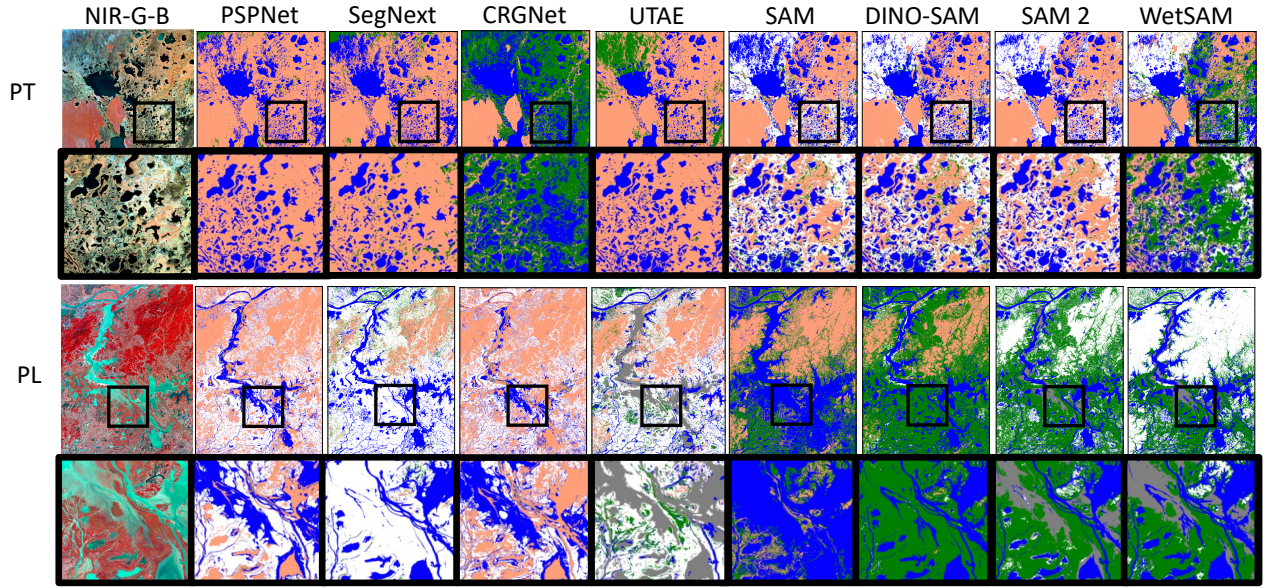
18

Figure 9: The visualization results of comparative studies.

Table 3: Ablation study of WetSAM across eight study regions (F1-score, %).

Region	w/o Temporal	w/o Spatial	w/o Align	w/o Adapter	w/o Time Emb.	Full Model
PL	76.42	82.51	83.15	81.36	83.45	84.07
MR	76.88	83.67	84.42	82.54	84.82	85.44
SD	85.31	85.92	86.51	84.72	86.94	87.61
SW	77.41	83.12	83.85	82.01	84.11	84.82
AM	84.15	85.14	85.92	84.12	86.05	86.87
BS	80.12	83.65	84.38	82.47	84.51	85.25
PT	74.16	82.94	83.75	81.85	83.92	84.74
BA	81.63	84.02	84.88	82.96	85.08	85.75
Average	79.51	83.87	84.61	82.75	84.86	85.58

it struggles with the satellite imagery and wetland scenarios. As reflected in Table 3, there is a performance degradation of 2.83% in average F1-score, which underscores the necessity of the multi-scale adapter in bridging the special knowledge gap and recalibrating features to distinguish different wetlands.

Rational for time embedding. To assess the role of temporal positional encoding, we remove the time embedding and relied solely on content-based attention. Without explicit time encoding, the model treats the time series as an unordered set of snapshots rather than an ordered sequence. Quantitatively, we observed a drop in F1-score to 84.86%, particularly in regions where phenological timing is crucial. This confirms that time embedding effectively guides the model to learn ordered hydrological patterns rather than relying on unordered spectral similarity alone.
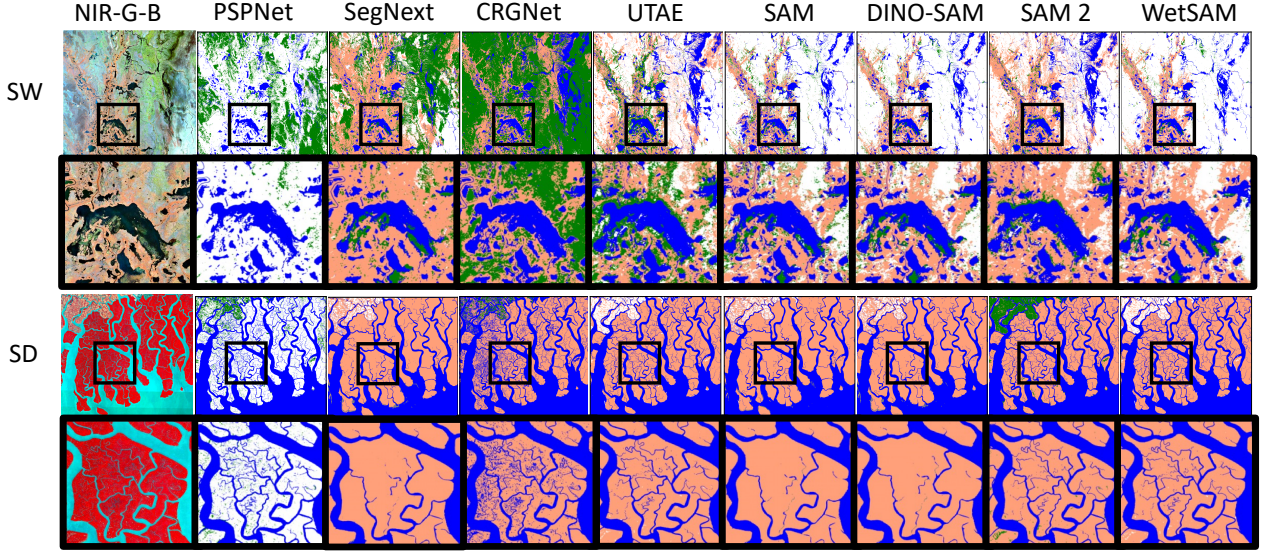
Figure 10: The visualization results of comparative studies.

6.2. Cross-region generalization

We further assess the generalization capability of WetSAM through a cross-region evaluation, in which the model is trained on seven regions and directly tested on one unseen regions without any fine-tuning. This experiment simulates real large-scale wetland mapping scenarios where annotated samples may not be available for all areas of interest.

As summarized in Table 4, WetSAM demonstrates superior robustness across all eight unseen test regions, achieving a stable average F1-score of 82.99%. Compared to the fully supervised setting, WetSAM exhibits a marginal average performance drop of 2.59%. In contrast, the traditional temporal model UTAE shows a significant performance collapse when applied to unseen regions with an average of 71.77%, indicating severe overfitting to site-specific features.

Notably, WetSAM outperforms the zero-shot capabilities of SAM 2 by 2.71% in average F1-score, particularly in ecologically complex regions like PT and PL. This consistent advantage confirms that WetSAM captures a more universal phenological trends that are shared across geographically distant wetland ecosystems. These results highlight WetSAM's potential as a reliable tool for zero-shot large-scale wetland monitoring in data-scarce regions.

Table 4: Cross-region generalization performance (F1-score, %). Each column represents the result when the corresponding region is used as the unseen test set, with the model trained on the remaining seven regions.

Method	PL	MR	SD	SW	AM	BS	PT	BA	Average
SAM	78.14	80.21	82.55	76.12	79.34	80.01	75.22	77.89	78.69
SAM 2	79.85	81.33	83.42	78.43	81.12	81.05	77.12	79.94	80.28
UTAE	71.24	73.56	75.12	69.84	72.45	73.18	67.54	71.22	71.77
WetSAM (Ours)	**81.82**	**83.14**	**85.41**	**81.25**	**84.52**	**83.37**	**80.84**	**83.56**	**82.99**

6.3. Sensitivity to temporal length

To investigate the influence of the input temporal length, we vary the number of time-series images fed into the temporal branch by adjusting the window length n from 1 to 12. Table 5 summarizes the results. In relatively stable regions such as SD and BS, the F1-score improves steadily with increasing n, as additional observations reinforce spectral stability and reduce noise from clouds or anomalous pixels. For highly seasonal regions such as PL and SW, the performance gain is even more pronounced when n increases from 1 to 6, averaging a 5.12% gain in F1-score. This is because a larger n allows the temporal aggregation module to more accurately model the long-term phenological trends and abrupt hydrological events. However, we observe that the marginal gains diminish beyond $n = 6$, with the improvement from $n = 9$ to $n = 12$ being less than 1%. This indicates that excessive temporal redundancy yields limited additional information once the primary seasonal cycles are sufficiently captured. Considering the trade-off between computational efficiency and segmentation accuracy, $n = 6$ to 12 appears to be an optimal range for large-scale wetland mapping using WetSAM.

Table 5: Performance comparison (F1-score, %) under different length of input time-series images (n) across all eight regions.

Region	$n = 1$	$n = 3$	$n = 6$	$n = 9$	$n = 12$ (**Full**)
PL	76.42	79.31	81.64	82.92	84.07
MR	76.88	79.52	82.81	84.73	85.44
SD	85.31	86.43	87.01	87.55	87.61
SW	77.41	79.89	82.43	83.11	84.82
AM	84.15	84.64	86.03	86.42	86.87
BS	80.12	82.08	84.24	84.69	85.25
PT	74.16	79.03	82.17	83.28	84.74
BA	81.63	82.54	84.22	85.19	85.75
Average	79.51	81.68	83.82	84.74	85.57

6.4. Sensitivity to label density

To evaluate the data efficiency of WetSAM, we investigate its performance under different densities of point-level annotations. Specifically, we randomly sample a subset of the original point labels at ratios of 10%, 30%, 50%, 70%, 90%, and 100% for training. For each ratio, the sampling process ensures that the labels are equally distributed and cover across all wetland types in each study region. As illustrated in Table 6, WetSAM demonstrates strong robustness even under extremely sparse supervision. With only 10% of the point labels, the model achieves a promising average F1-score of 79.60%. This performance is already comparable to several baseline methods trained on much denser information, indicating that the prompt-adapted SAM backbone provides a strong structural prior that effectively compensates for the scarcity of supervision.

We observe that the performance gains are most pronounced as the label ratio increases from 10% to 50%, with the average F1-score rising from 79.60% to 83.87%. Beyond the 70% threshold, the improvement curve exhibits a distinct saturation effect. Specifically, increasing the label density from 70% to 100% yields only a marginal gain of 0.90% in the average F1-score. This suggests that WetSAM can effectively capture the

core phenological and spatial characteristics of wetlands using only a limited fraction of available annotations. This high data efficiency is particularly valuable for large-scale wetland mapping, as it significantly reduces the human labor required for ground-truth collection while maintaining high segmentation accuracy.

Table 6: Performance comparison (F1-score, %) under different percentages of point-level annotations across all eight regions.

Region	10%	30%	50%	70%	90%	100%
PL	76.87	81.20	83.27	83.68	83.90	84.07
MR	79.21	82.64	83.72	84.51	85.34	85.44
SD	83.40	85.97	86.51	87.42	87.59	87.61
SW	78.62	81.07	82.79	83.62	84.38	84.82
AM	81.67	83.51	84.98	86.07	86.65	86.87
BS	80.05	82.42	83.33	84.14	84.79	85.25
PT	77.46	80.94	82.69	83.44	84.01	84.74
BA	79.51	81.93	83.66	84.51	85.23	85.75
Average	79.60	82.46	83.87	84.67	85.24	85.57

6.5. Sensitivity to label noise

In practice, wetland point annotations are possible to be subject to errors due to the spectral similarities between classes or seasonal shifts. To evaluate the fault tolerance of WetSAM, we introduce random label noise at ratios from 5% to 60%. As demonstrated in Table 7, WetSAM maintains a stable performance when the noise ratio is within 25%. The average F1-score only experiences a negligible decrease of 1.96% (from 85.43% to 83.47%). However, a sharp drop in performance is observed once the noise exceeds the 30% threshold, where the erroneous signals begin to overwhelm the true labels. Notably, seasonal regions (e.g., PL, PT, and SW) exhibit much higher sensitivity to extreme noise compared to stable regions. In these dynamic environments, high noise ratios lead to a failure in temporal modeling, causing the F1-score to plunge by over 20% as the noise moves from 30% to 50%. In contrast, stable regions like SD and AM show a more buffered degradation. These results suggest that while WetSAM is highly robust to moderate errors, maintaining label accuracy remains crucial in complex environments.

Table 7: Robustness analysis of WetSAM under different label noise levels (5% to 60%). "Seasonal" regions (PL, MR, SW, PT) exhibit higher sensitivity to noise beyond the 30% threshold.

Region	5%	10%	15%	20%	25%	30%	40%	50%	60%
PL	83.91	83.82	83.65	82.25	82.88	75.12	62.34	50.15	41.22
MR	85.24	85.15	84.98	83.64	84.15	77.34	64.88	53.42	44.15
SD	87.55	87.48	87.31	86.11	86.82	82.45	74.12	66.89	58.42
SW	84.65	84.51	84.32	82.98	83.45	76.05	63.15	51.27	42.06
AM	86.75	86.62	86.44	85.16	85.91	81.82	73.54	65.14	57.21
BS	85.11	85.02	84.88	83.57	84.22	79.76	71.22	63.45	55.33
PT	84.58	84.44	84.18	82.79	83.21	75.43	61.92	49.85	40.54
BA	85.62	85.54	85.35	84.06	84.76	80.12	72.43	64.91	56.12
Average	85.43	85.32	85.14	84.79	83.47	78.51	68.08	58.14	49.38

6.6. Limitations

Despite the promising performance of WetSAM in weakly supervised wetland mapping, several limitations remain to be addressed in future research. First, the reliance on optical satellite imagery renders the framework susceptible to atmospheric conditions. Although we apply strict cloud filtering, persistent cloud cover in tropical or monsoon-dominated regions can still disrupt the continuity of time series. Integrating All-Weather Synthetic Aperture Radar (SAR) data into the framework to compensate for optical data gaps represents a critical direction for improvement. Second, while WetSAM demonstrates robustness to moderate label noise, our robustness analysis reveals a performance bottleneck under high-noise conditions. This suggests that the correctness of the initial sparse prompts is needed to guide the learning of complex temporal patterns. Third, to leverage the structural priors of the foundation model, we freeze the image encoder of SAM during training. While the hierarchical adapter effectively bridges the domain gap, the frozen backbone may still limit the model's ability to learn features that are fundamentally different from natural images, specifically when extending the framework to other data modalities such as SAR data.

These limitations directly point to several future directions for our future work. First, to mitigate the impact of cloud cover and data gaps in optical imagery, it is necessary to extend the framework to support multi-modal data fusion, specifically by integrating Sentinel-1 SAR data to enable all-weather wetland monitoring. Second, label quality is important; therefore, we aim to construct a reliable global wetland sample database using automatic ways. Finally, we envision exploring parameter-efficient fine-tuning strategies to align the foundation model's representation space with the specific spectral characteristics of multi-modal remote sensing data.

7. Conclusion

In this study, we proposed WetSAM, a novel dual-branch framework designed to address the critical challenge of accurate wetland mapping under extremely sparse point-level supervision. By extending the Segment Anything Model (SAM) with a hierarchical multi-scale adapter and a dynamic temporal aggregation module, WetSAM successfully bridges the gap between static foundation models and dynamic satellite image time series. The proposed framework effectively synergizes temporal and spatial information: the temporal branch leverages phenological trends to resolve spectral ambiguities, while the spatial branch reconstructs coherent boundaries via a temporal-constrained region-growing strategy. A bidirectional prediction alignment further ensures that these two complementary views mutually reinforce each other, resulting in robust segmentation. Extensive experiments across eight geographically and ecologically diverse wetland regions demonstrate the superiority of our approach. WetSAM consistently outperforms state-of-the-art baselines, achieving an average F1-score of 85.58% and demonstrating remarkable stability even in highly seasonal environments. Crucially, our results highlight the framework's data efficiency; it retains high performance even when trained with only 70% of the available point annotations, making it a practical solution for large-scale applications where ground truth is scarce. Overall, WetSAM offers a scalable, cost-effective pathway for large-scale wetland monitoring, contributing to better conservation and management of the world's vital wetland resources. In the future, we

plan to incorporate multi-modal data fusion, particularly integrating SAR data for all-weather monitoring. We also aim to enhance the model's adaptability by exploring parameter-efficient fine-tuning strategies to unfreeze the image encoder, thereby better aligning the backbone with remote sensing domains.

References

Ali, M., Wu, T., Hu, H., Luo, Q., Xu, D., Zheng, W., Jin, N., Yang, C., & Yao, J. (2025). A review of the segment anything model (sam) for medical image analysis: Accomplishments and perspectives. *Computerized Medical Imaging and Graphics*, *119*, 102473.

Ashok, A., Rani, H. P., & Jayakumar, K. (2021). Monitoring of dynamic wetland changes using ndvi and ndwi based landsat imagery. *Remote Sensing Applications: Society and Environment*, *23*, 100547.

Carion, N., Gustafson, L., Hu, Y.-T., Debnath, S., Hu, R., Suris, D., Ryali, C., Alwala, K. V., Khedr, H., Huang, A. et al. (2025). Sam 3: Segment anything with concepts. *arXiv preprint arXiv:2511.16719*, .

Chan, S., Zhou, W., Lei, Y., Li, C., Hu, J., & Hong, F. (2025). Sparse point annotations for remote sensing image segmentation. *Scientific Reports*, *15*, 27347.

Chen, T., Zhu, L., Deng, C., Cao, R., Wang, Y., Zhang, S., Li, Z., Sun, L., Zang, Y., & Mao, P. (2023). Sam-adapter: Adapting segment anything in underperformed scenes. In *Proceedings of the IEEE/CVF International Conference on Computer Vision* (pp. 3367–3375).

Chung, J., Gulcehre, C., Cho, K., & Bengio, Y. (2014). Empirical evaluation of gated recurrent neural networks on sequence modeling. *arXiv preprint arXiv:1412.3555*, .

Cleveland, R. B., Cleveland, W. S., McRae, J. E., Terpenning, I. et al. (1990). Stl: A seasonal-trend decomposition. *J. off. Stat*, *6*, 3–73.

Dong, Z., Wang, Z., Liu, D., Song, K., Li, L., Jia, M., & Ding, Z. (2014). Mapping wetland areas using landsat-derived ndvi and lswi: A case study of west songnen plain, northeast china. *Journal of the Indian Society of Remote Sensing*, *42*, 569–576.

Dronova, I. (2015). Object-based image analysis in wetland research: A review. *Remote Sensing*, *7*, 6380–6413.

Dronova, I., Gong, P., Wang, L., & Zhong, L. (2015). Mapping dynamic cover types in a large seasonally flooded wetland using extended principal component analysis and object-based classification. *Remote Sensing of Environment*, *158*, 193–206.

Erwin, K. L. (2009). Wetlands and global climate change: the role of wetland restoration in a changing world. *Wetlands Ecology and management*, *17*, 71–84.

Garnot, V. S. F., & Landrieu, L. (2021). Panoptic segmentation of satellite image time series with convolutional temporal attention networks. In *Proceedings of the IEEE/CVF International Conference on Computer Vision* (pp. 4872–4881).

Gong, P., Niu, Z., Cheng, X., Zhao, K., Zhou, D., Guo, J., Liang, L., Wang, X., Li, D., Huang, H. et al. (2010). China's wetland change (1990–2000) determined by remote sensing. *Science China Earth Sciences*, *53*, 1036–1042.

Guirado, E., Blanco-Sacristan, J., Rodriguez-Caballero, E., Tabik, S., Alcaraz-Segura, D., Martinez-Valderrama, J., & Cabello, J. (2021). Mask r-cnn and obia fusion improves the segmentation of scattered vegetation in very high-resolution optical sensors. *Sensors*, *21*, 320.

Guo, M.-H., Lu, C.-Z., Hou, Q., Liu, Z., Cheng, M.-M., & Hu, S.-M. (2022). Segnext: Rethinking convolutional attention design for semantic segmentation. *Advances in neural information processing systems*, *35*, 1140–1156.

Hong, D., He, W., Yokoya, N., Yao, J., Gao, L., Zhang, L., Chanussot, J., & Zhu, X. (2021). Interpretable hyperspectral artificial intelligence: When nonconvex modeling meets hyperspectral remote sensing. *IEEE Geoscience and Remote Sensing Magazine*, *9*, 52–87.

Hosseiny, B., Mahdianpari, M., Brisco, B., Mohammadimanesh, F., & Salehi, B. (2021). Wetnet: A spatial–temporal ensemble deep learning model for wetland classification using sentinel-1 and sentinel-2. *IEEE transactions on geoscience and remote sensing*, *60*, 1–14.

Hu, S., Niu, Z., & Chen, Y. (2017). Global wetland datasets: a review. *Wetlands*, *37*, 807–817.

Hua, Y., Marcos, D., Mou, L., Zhu, X. X., & Tuia, D. (2021). Semantic segmentation of remote sensing images with sparse annotations. *IEEE Geoscience and Remote Sensing Letters*, *19*, 1–5.

Jamali, A., & Mahdianpari, M. (2022). Swin transformer and deep convolutional neural networks for coastal wetland classification using sentinel-1, sentinel-2, and lidar data. *Remote Sensing*, *14*, 359.

Jamali, A., Mahdianpari, M., Brisco, B., Mao, D., Salehi, B., & Mohammadimanesh, F. (2022). 3dunetgsformer: A deep learning pipeline for complex wetland mapping using generative adversarial networks and swin transformer. *Ecological informatics*, *72*, 101904.

Jing, L., Zhou, Y., Zeng, Q., Liu, S., Lei, G., Lu, C., & Wen, L. (2020). Exploring wetland dynamics in large river floodplain systems with unsupervised machine learning: A case study of the dongting lake, china. *Remote Sensing*, *12*, 2995.

Kirillov, A., Mintun, E., Ravi, N., Mao, H., Rolland, C., Gustafson, L., Xiao, T., Whitehead, S., Berg, A. C., Lo, W.-Y. et al. (2023). Segment anything. In *Proceedings of the IEEE/CVF international conference on computer vision* (pp. 4015–4026).

Li, Z., Zhang, X., & Xiao, P. (2022). Spectral index-driven fcn model training for water extraction from multispectral imagery. *ISPRS Journal of Photogrammetry and Remote Sensing*, *192*, 344–360.

Lin, Y., Shen, M., Liu, B., & Ye, Q. (2013). Remote sensing classification method of wetland based on an improved svm. *The International Archives of the Photogrammetry, Remote Sensing and Spatial Information Sciences*, *40*, 179–183.

Liu, N., Xu, X., Su, Y., Zhang, H., & Li, H.-C. (2025). Pointsam: Pointly-supervised segment anything model for remote sensing images. *IEEE Transactions on Geoscience and Remote Sensing*, .

Ma, J., He, Y., Li, F., Han, L., You, C., & Wang, B. (2024). Segment anything in medical images. *Nature Communications*, *15*, 654.

Ma, Y., Zhou, Z., She, X., Zhou, L., Ren, T., Liu, S., & Lu, J. (2022). Identifying dike-pond system using an improved cascade r-cnn model and high-resolution satellite images. *Remote Sensing*, *14*, 717.

Mahdianpari, M., Salehi, B., Mohammadimanesh, F., & Motagh, M. (2017). Random forest wetland classification using alos-2 l-band, radarsat-2 c-band, and terrasar-x imagery. *ISPRS Journal of Photogrammetry and Remote Sensing*, *130*, 13–31.

Marjani, M., Mohammadimanesh, F., Mahdianpari, M., & Gill, E. W. (2025). A novel spatio-temporal vision transformer model for improving wetland mapping using multi-seasonal sentinel data. *Remote Sensing Applications: Society and Environment*, *37*, 101401.

Murray, N. J., Phinn, S. R., DeWitt, M., Ferrari, R., Johnston, R., Lyons, M. B., Clinton, N., Thau, D., & Fuller, R. A. (2019). The global distribution and trajectory of tidal flats. *Nature*, *565*, 222–225.

Pattison-Williams, J. K., Pomeroy, J. W., Badiou, P., & Gabor, S. (2018). Wetlands, flood control and ecosystem services in the smith creek drainage basin: A case study in saskatchewan, canada. *Ecological economics*, *147*, 36–47.

Pouliot, D., Latifovic, R., Pasher, J., & Duffe, J. (2019). Assessment of convolution neural networks for wetland mapping with landsat in the central canadian boreal forest region. *Remote Sensing*, *11*, 772.

Ravi, N., Gabeur, V., Hu, Y.-T., Hu, R., Ryali, C., Ma, T., Khedr, H., Rädle, R., Rolland, C., Gustafson, L. et al. (2024). Sam 2: Segment anything in images and videos. *arXiv preprint arXiv:2408.00714*, .

Ruan, R., & Ustin, S. (2012). Mapping of freshwater lake wetlands using object-relations and rule-based inference. *Chinese geographical science*, *22*, 462–471.

Sidike, P., Sagan, V., Maimaitijiang, M., Maimaitiyiming, M., Shakoor, N., Burken, J., Mockler, T., & Fritschi, F. B. (2019). dpen: Deep progressively expanded network for mapping heterogeneous agricultural landscape using worldview-3 satellite imagery. *Remote sensing of environment*, *221*, 756–772.

Subhani, M. N. (2025). Resam: Refine, requery, and reinforce: Self-prompting point-supervised segmentation for remote sensing images. *arXiv preprint arXiv:2511.21606*, .

Team, W. D. (2025). 30 m Global Near-Daily Wetland Dynamics (2013-2024). Available at `https://doi.org/10.12436/GWD30.60.20250703`. URL: `https://doi.org/10.12436/GWD30.60.20250703`. doi:10.12436/GWD30.60.20250703 dataset.

Wang, D., Zhang, J., Du, B., Xu, M., Liu, L., Tao, D., & Zhang, L. (2023a). Samrs: Scaling-up remote sensing segmentation dataset with segment anything model. *Advances in Neural Information Processing Systems*, *36*, 8815–8827.

Wang, M., Mao, D., Wang, Y., Li, H., Zhen, J., Xiang, H., Ren, Y., Jia, M., Song, K., & Wang, Z. (2024). Interannual changes of urban wetlands in china's major cities from 1985 to 2022. *ISPRS Journal of Photogrammetry and Remote Sensing*, *209*, 383–397.

Wang, M., Mao, D., Wang, Y., Xiao, X., Xiang, H., Feng, K., Luo, L., Jia, M., Song, K., & Wang, Z. (2023b). Wetland mapping in east asia by two-stage object-based random forest and hierarchical decision tree algorithms on sentinel-1/2 images. *Remote Sensing of Environment*, *297*, 113793.

Xu, P., Niu, Z., & Tang, P. (2018). Comparison and assessment of ndvi time series for seasonal wetland classification. *International Journal of Digital Earth*, *11*, 1103–1131.

Xu, Y., & Ghamisi, P. (2022). Consistency-regularized region-growing network for semantic segmentation of urban scenes with point-level annotations. *IEEE Transactions on Image Processing*, *31*, 5038–5051.

Yan, Z., Li, J., Li, X., Zhou, R., Zhang, W., Feng, Y., Diao, W., Fu, K., & Sun, X. (2023). Ringmo-sam: A foundation model for segment anything in multimodal remote-sensing images. *IEEE Transactions on Geoscience and Remote Sensing*, *61*, 1–16.

Yuan, S., Chen, S., Lin, T., Yuan, J., Tian, G., Xu, Y., Wang, J., & Gong, P. (2025a). Dynamic mapping from static labels: remote sensing dynamic sample generation with temporal-spectral embedding. *arXiv preprint arXiv:2506.02574*, .

Yuan, S., Liang, X., Lin, T., Chen, S., Liu, R., Wang, J., Zhang, H., & Gong, P. (2025b). A comprehensive review of remote sensing in wetland classification and mapping. *arXiv preprint arXiv:2504.10842*, .

Yuan, S., Zhang, L., Dong, R., Xiong, J. et al. (2024). Relational part-aware learning for complex composite object detection in high-resolution remote sensing images. *IEEE Transactions on Cybernetics*, .

Zamboni, P. A. P., Blanch, X., Marcato Junior, J., Gonçalves, W. N., & Eltner, A. (2025). Do we need to label large datasets for river water segmentation? benchmark and stage estimation with minimum to non-labeled image time series. *International Journal of Remote Sensing*, *46*, 2719–2747.

Zhang, C., Han, D., Qiao, Y., Kim, J. U., Bae, S.-H., Lee, S., & Hong, C. S. (2023a). Faster segment anything: Towards lightweight sam for mobile applications. *arXiv preprint arXiv:2306.14289*, .

Zhang, C., Liu, L., Cui, Y., Huang, G., Lin, W., Yang, Y., & Hu, Y. (2023b). A comprehensive survey on segment anything model for vision and beyond. *arXiv preprint arXiv:2305.08196*, .

Zhang, T., Ren, Y., Li, W., Qin, C., Jiao, L., & Su, H. (2025). Csw-sam: a cross-scale algorithm for very-high-resolution water body segmentation based on segment anything model 2. *ISPRS Journal of Photogrammetry and Remote Sensing*, *228*, 208–227.

Zhang, X., Liu, L., Zhao, T., Wang, J., Liu, W., & Chen, X. (2024). Global annual wetland dataset at 30 m with a fine classification system from 2000 to 2022. *Scientific Data*, *11*, 310.

Zhang, Z., Fluet-Chouinard, E., Jensen, K., McDonald, K., Hugelius, G., Gumbricht, T., Carroll, M., Prigent, C., Bartsch, A., & Poulter, B. (2021). Development of the global dataset of wetland area and dynamics for methane modeling (wad2m). *Earth System Science Data*, *13*, 2001–2023.

Zhao, H., Shi, J., Qi, X., Wang, X., & Jia, J. (2017). Pyramid scene parsing network. In *Proceedings of the IEEE conference on computer vision and pattern recognition* (pp. 2881–2890).

Zhou, X., Liang, F., Chen, L., Liu, H., Song, Q., Vivone, G., & Chanussot, J. (2024). Mesam: Multiscale enhanced segment anything model for optical remote sensing images. *IEEE Transactions on Geoscience and Remote Sensing*, *62*, 1–15.